Journal of Materials Chemistry A

PAPER

View Article Online
View Journal | View Issue

Cite this: J. Mater. Chem. A, 2017, 5, 12400

High-performance ternary polymer solar cells from a structurally similar polymer alloy†

Wenfei Shen,[ab] Weichao Chen,[*ab] Dangqiang Zhu,[a] Jidong Zhang,[d] Xiaofeng Xu,[c] Huanxiang Jiang,[a] Ting Wang,[a] Ergang Wang[*c] and Renqiang Yang[*a]

Received 3rd April 2017
Accepted 19th May 2017

DOI: 10.1039/c7ta02891a

rsc.li/materials-a

High-efficiency ternary polymer solar cells (PSCs) are fabricated by using two donor polymers (PBDTTPD and PBDTTT-C-T) with similar polymer backbones and complementary absorption and $PC_{71}BM$ as the acceptor. A high power conversion efficiency (PCE) of 9.3% is achieved with a high short-circuit current density (J_{sc}) of 17.2 mA cm^{-2}. The enhanced J_{sc} and PCEs are mainly attributed to the broadened photoresponse of the ternary blend. Good miscibility of the two donor polymers is found due to the similar polymer main chains, leading to the desired morphology between the donors and $PC_{71}BM$ in the ternary blends. The trend of open-circuit voltage (V_{oc}) variations indicates the formation of a polymer alloy in this ternary blend. Our work demonstrates that using two donor polymers with similar backbone structures is a rational strategy for realizing high-performance ternary PSCs.

1. Introduction

Polymer solar cells (PSCs) have received tremendous attention in the last ten years due to their advantages of low cost, light weight, and 珑exibility.[1–5] So far, single bulk-heterojunction (BHJ) PSCs have achieved power conversion efficiencies (PCEs) over 11% by using new conjugated polymers and fullerene derivatives,[6–10] as well as novel fabrication techniques.[1,4,8,11–17] However, the relatively narrow absorption widths of the active layers of PSCs as compared to inorganic solar cells,[18–20] is one of the key limiting factors for further improvement of the photocurrent and PCE of PSCs.[4,21] Therefore, it is essential to enhance the light harvesting of PSCs by using active layers that can efficiently cover the solar spectrum with high absorption coef-珑cients.[18,19] One approach is to design low band gap materials with broad absorption spectra to match the solar spectrum, but few successful examples have been found so far.[8,9] On the other hand, tandem solar cells consisting of two sub-cells with complementary absorption in each sub-cell are proposed therea沢er to realize broad photon harvesting relative to single-junction solar cells.[4,12,13,22] However, it is complicated and uneconomical to join two sub-cells in series by using interconnecting layers.

Recently, employing ternary solar cells containing three photo-active materials (two donors with one acceptor, or one donor with two acceptors) with complementary absorption has emerged as an attractive strategy to enhance light harvesting.[14,16,18,23–49] They combine the advantages of the broadened photoresponse of tandem solar cells and the easily solution-processed fabrication of single junction PSCs. For ternary solar cells, the incorporation of the third component in ternary PSCs should enhance the light harvest without limiting exciton dissociation and charge transport and collection.[24,25,33,50] Therefore, the morphology of the ternary blend plays a critical role in the overall device performance, where continuous interpenetrating networks with nanoscale phase separation are favourable.[33,35] However, it is evident that the third component usually disturbs the initial orientation of the materials in the binary blend.[24,36] Especially, in a ternary blend with two donor polymers, each polymer has its own preferred orientation that is strongly correlated with the polymer structures. The miscibility of the two polymers could strongly affect the blend morphology and the 珋nal photovoltaic performance of the ternary system. We note that some efficient ternary polymer solar cells were based on two donor polymers with different structures.[51–53] In contrast, several reports revealed that the chemical structures of donor materials can strongly in珞uence the physical properties such as the molecular orientation and crystallinity. Using two donor polymers with more compatible structures may lead to less interference and form more desired microstructures in the active layer.[54] To further study this controversy, more ternary

[a]CAS Key Laboratory of Bio-based Materials, Qingdao Institute of Bioenergy and Bioprocess Technology, Chinese Academy of Sciences, Qingdao 266101, China. E-mail: yangrq@qibebt.ac.cn
[b]College of Textiles & Clothing, Qingdao University, Qingdao266071, China. E-mail: chenwc@qibebt.ac.cn
[c]Department of Chemical and Chemical Engineering/Polymer Technology, Chalmers University of Technology, SE-412 96, Göteborg, Sweden. E-mail: ergang@chalmers.se
[d]State Key Laboratory of Polymer Physics and Chemistry, Changchun Institute of Applied Chemistry, Chinese Academy of Sciences, Changchun 130022, China

† Electronic supplementary information (ESI) available. See DOI: 10.1039/c7ta02891a

systems should be investigated, which is also one of the key concerns in this work. Apart from the morphology, suitable energy level alignment is also of importance for determining the exciton dissociation, charge transport, and open-circuit voltage (V_{oc}) in ternary blend systems.[28,30,35] In brief, a suitable combination of donor polymers with complementary absorption, desired energy levels and good miscibility is essential to boost the performance of a ternary system.[18]

In this work, we choose poly([4,8-bis-(2-ethyl-hexyl-thiophene-5-yl)-benzo[1,2-*b*:4,5-*b*^{0}]dithiophene-2,6-diyl]-alt-[2-(2^0-ethyl-hexanoyl)-thieno[3,4-*b*]thiophen-4,6-diyl])(PBDTTT-C-T) and poly(benzo[1,2-*b*:4,5-*b*^{0}]dithiophene-alt-thieno[3,4-*c*]pyrrole-4,6-dione) (PBDTTPD) as donors, and phenyl-C_{71}-butyric acid methyl ester ($PC_{71}BM$) as the acceptor to realize high-performance ternary PSCs. PBDTTT-C-T and PBDTTPD feature similar polymer backbones, which tend to form good miscibility in the ternary blend. Well-mixed polymer phases and $PC_{71}BM$ is observed without large phase separation. Associated with the complementary absorption and cascade energy levels, the ternary PSC attains a high PCE of 9.3% with a decent J_{sc} of 17.18 mA cm^{-2}.

2. Results and discussion

The chemical structures of PBDTTPD, PBDTTT-C-T and $PC_{71}BM$ are depicted in Fig. 1a. The two donor polymers show similar structures where both of them have dibenzothiophene (BDT) and fused thiophene moieties in their backbones. This may promise good compatibility in the ternary blend 珡lms and form an appropriate morphology.[34,35] In addition, PBDTTT-C-T and PBDTTPD present complementary absorption in thin 珡lms. As shown in Fig. 1b, PBDTTPD exhibits strong absorption in the range of 400–650 nm, whereas the major absorption band for the PBDTTT-C-T 珡lm is located from 600 to 750 nm. Thus, an enhanced photocurrent can be expected due to the broad photoresponse in the ternary blend. The absorption spectra of the ternary blends with different weight ratios are depicted in Fig. 2.

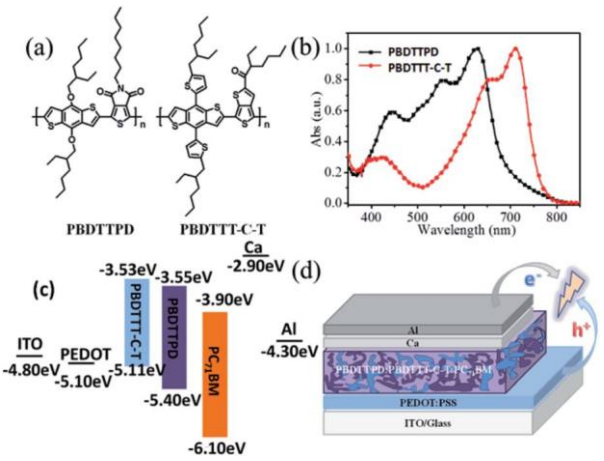

Fig. 1 (a) Chemical structures of PBDTTPD, PBDTTT-C-T and $PC_{71}BM$. (b) Absorption spectra of PBDTTPD and PBDTTT-C-T in thin films. (c) Energy level diagram of PBDTTPD, PBDTTT-C-T and $PC_{71}BM$. (d) Schematic diagram of the ternary solar cells.

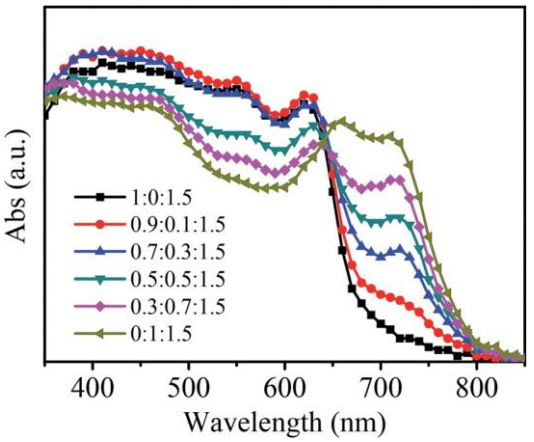

Fig. 2 Absorption spectra of the blend films with different PBDTTPD:PBDTTT-C-T:$PC_{71}BM$ weight ratios.

The absorption intensities gradually increase in the range of 650–800 nm when increasing the content of PBDTTT-C-T. This reveals that the incorporation of PBDTTT-C-T effectively broadens the absorption of the ternary blends.[18]

The energy levels of PBDTTT-C-T exhibit a good match with those of PBDTTPD and $PC_{71}BM$.[26] As shown in Fig. 1c, this ternary system features a cascade energy level alignment. The energy levels of the highest occupied molecular orbital (HOMO) and the lowest unoccupied molecular orbital (LUMO) of PBDTTT-C-T and PBDTTPD are —5.11 eV and —5.40 eV, and —3.55 eV and —3.53 eV, respectively. The LUMO–LUMO offset of each donor and $PC_{71}BM$ (0.35 and 0.37 eV) is appropriate for exciton dissociation in ternary blend PSCs.[33] Therefore, PBDTTT-C-T is an appropriate second donor to improve the performance of ternary blend PSCs.

The ternary PSCs were fabricated by using the device structure of glass/ITO/PEDOT:PSS/PBDTTPD:PBDTTT-C-T:$PC_{71}BM$/Ca/Al (Fig. 1d). The solar cells were measured under an illumination of AM 1.5G simulated solar light at 100 mW cm^{-2}. The fabrication of the solar cells was optimized by varying the D : A weight ratio, active layer thickness and solvent additive, and the detailed fabrication processes are illustrated in the experimental section. The optimal 珡lm thicknesses of the active layers were around 100 nm. The typical current density–voltage (J–V) curves are shown in Fig. 3a and the corresponding device parameters are summarized in Table 1. Binary solar cells based on PBDTTPD:$PC_{71}BM$ and PBDTTT-C-T:$PC_{71}BM$ were also fabricated as a reference. The binary PSC based on PBDTTPD:$PC_{71}BM$ exhibits an average PCE of 7.34%, with a V_{oc} of 0.92 V, a J_{sc} of 12.80 mA cm^{-2} and a FF of 0.62. The PBDTTT-C-T:$PC_{71}BM$ shows a PCE of 7.29%, with a lower V_{oc} of 0.76 V, a J_{sc} of 14.71 mA cm^{-2} and a comparable FF of 0.65. The device performance of the two binary solar cells is consistent with the reports in the literature.[39,55] Compared to the binary solar cells, the ternary solar cells exhibit enhanced PCEs when using a lower content of PBDTTT-C-T than PBDTTPD in the ternary blends (PBDTTPD:PBDTTT-C-T:$PC_{71}BM$ of 0.9 : 0.1 : 1.5, 0.7 : 0.3 : 1.5 and 0.5 : 0.5 : 1.5), whereas the PCEs of the ternary solar cells decrease when the content of PBDTTT-C-T becomes

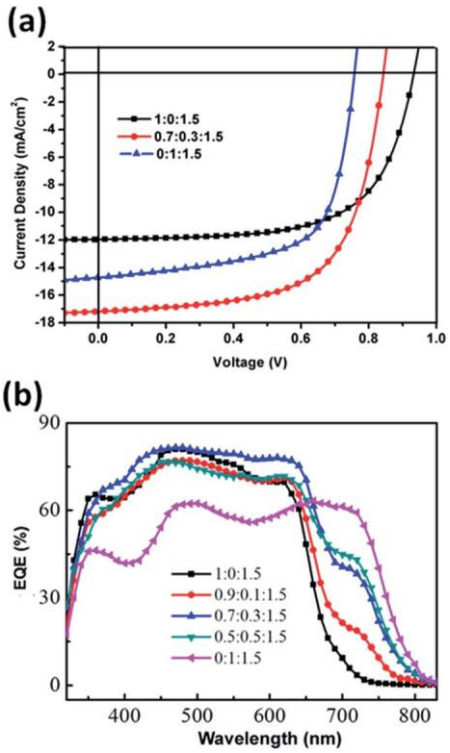

Fig. 3 (a) *J*–*V* curves of the solar cells with different PBDTTPD:PBDTTT-C-T:$PC_{71}BM$ weight ratios. (b) The corresponding EQE spectra of the solar cells.

higher than that of PBDTTT-C-T (0.3 : 0.7 : 1.5 and 0.1 : 0.9 : 1.5). In this case, the maximum PCE of 9.27% is observed with the content ratio of 0.7 : 0.3 : 1.5, with a V_{oc} of 0.84 V, a J_{sc} of 17.18 mA cm^{-2} and a FF of 0.64. The enhanced PCE is mainly due to the increased J_{sc}, which stems from the extended light adsorption. In addition, the V_{oc} of the ternary devices is not limited by the lower value of the two binary PSCs, but remains between the two extremes with a D : A ratio dependence. It increases with the content of PBDTTPD in the ternary blends. Similar V_{oc} variations were found in some other ternary systems, indicating the formation of an alloy structure of the two donor polymers.[16,24]

The external quantum efficiency (EQE) was measured to investigate the effect of PBDTTT-C-T on the photoresponse of the ternary PSCs. As shown in Fig. 3b, the ternary solar cells show a broader photoresponse in the wavelength region of 300–800 nm, as compared to the PBDTTPD:$PC_{71}BM$ binary solar cell. The enhanced photoresponse mainly originates from the contribution of PBDTTT-C-T, since PBDTTT-C-T shows the primary absorption in the wavelength region of 650–800 nm.[23] In addition, the incorporation of PBDTTT-C-T retains the EQE profiles of the PBDTTPD:$PC_{71}BM$ binary solar cell. Therefore, PBDTTT-C-T plays an effective role in the improvement of J_{sc} in this ternary system. The maximum EQE of around 80% was obtained at the 30% PBDTTT-C-T content. The J_{sc} values calculated from the EQE curves and solar spectra are in good agreement with the measured J_{sc} from the *J*–*V* curves with a mismatch of less than 5%.

The charge transport properties of the binary and ternary PSCs were investigated by the space-charge-limited-current (SCLC) method. The device structure and calculations are described in the ESI.† The hole mobility (μ_h) and electron mobility (μ_e) of the PSCs are summarized in Table 2. The optimal ternary PSC with a content ratio of 0.7 : 0.3 : 1.5 shows well balanced hole and electron transport mobility, which may be beneficial for suppressing the bimolecular recombination and improving the photocurrent.[43] Moreover, the balanced charge transport can also help to reduce the space-charge effect, all of which synergistically improve the FF up to 0.64.[33,36]

The surface morphologies of the binary and ternary blend films were investigated by atomic force microscopy (AFM). As shown in Fig. 4a and c, the binary blend films of PBDTTPD:$PC_{71}BM$ and PBDTTT-C-T:$PC_{71}BM$ present low surface roughness with a root-mean-square (RMS) below 3 nm, where both of the surfaces are composed of small grains, which can be clearly observed in the phase images (Fig. 4d and f). When 30% of PBDTTT-C-T is incorporated, the ternary blend film shows a similar surface morphology to that of the binary blend films with a comparable RMS of 3.2 nm (Fig. 4b and e). These results indicated that incorporating 30% of PBDTTT-C-T has little influence on the morphology of the ternary blend.

Table 2 The hole and electron mobilities of the blends measured by the SCLC method

Devices	μ_h [$cm^2 V^{-1} s^{-1}$]	μ_e [$cm^2 V^{-1} s^{-1}$]	μ_h/μ_e
1 : 0 : 1.5	2.15×10^{-4}	1.75×10^{-4}	1.23
0.7 : 0.3 : 1.5	1.98×10^{-4}	1.99×10^{-4}	0.99
0 : 1 : 1.5	2.16×10^{-4}	1.47×10^{-4}	1.47

Table 1 Photovoltaic parameters of the solar cells

D1 : D2 : $PC_{71}BM$[a]	V_{oc}[b] [V]	J_{sc}[b] [mA cm^{-2}]	FF[b]	PCE[b] [%]
1 : 0 : 1.5	0.92 ± 0.01	12.80 ± 0.13 (12.30)[c]	0.62 ± 0.01	7.34 ± 0.22
0.9 : 0.1 : 1.5	0.85 ± 0.02	15.17 ± 0.24 (14.89)	0.61 ± 0.01	7.87 ± 0.25
0.7 : 0.3 : 1.5	0.84 ± 0.01	17.18 ± 0.19 (17.02)	0.64 ± 0.01	9.27 ± 0.13
0.5 : 0.5 : 1.5	0.83 ± 0.01	16.19 ± 0.32 (15.96)	0.65 ± 0.02	8.77 ± 0.16
0.3 : 0.7 : 1.5	0.82 ± 0.02	14.56 ± 0.25 (14.23)	0.59 ± 0.01	7.03 ± 0.36
0.1 : 0.9 : 1.5	0.81 ± 0.02	14.39 ± 0.21 (14.04)	0.56 ± 0.02	6.54 ± 0.13
0 : 1 : 1.5	0.76 ± 0.01	14.71 ± 0.47 (14.23)	0.65 ± 0.02	7.29 ± 0.24

[a] D1 is PBDTTPD, D2 is PBDTTT-C-T. [b] Standard deviations obtained from 15 devices. [c] Calculated J_{sc} from the EQE spectra.

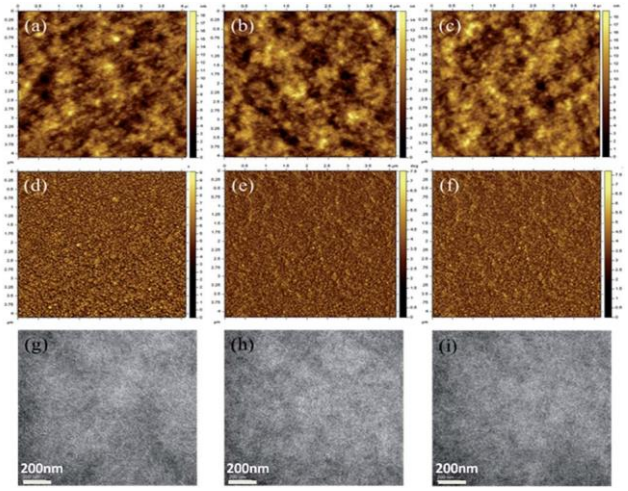

Fig. 4 AFM height images of the (a) PBDTTPD:$PC_{71}BM$ (1 : 1.5) blend film, (b) PBDTTPD:PBDTTT-C-T:$PC_{71}BM$ (0.7 : 0.3 : 1.5) blend film and (c) PBDTTT-C-T:$PC_{71}BM$ (1 : 1.5) blend film. (d), (e) and (f) are the corresponding phase images, respectively; (g), (h) and (i) are the corresponding TEM images, respectively.

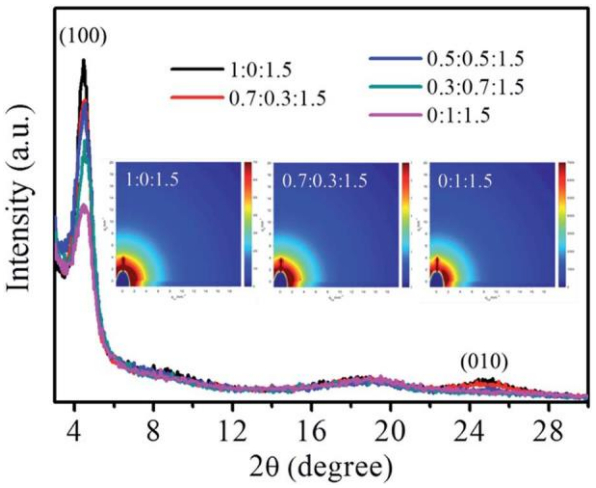

Fig. 5 XRD curves of the blend films. The inset images are the 2D GIWAXS images of the blend films.

珡lms. No large domains can be found in the ternary blend, indicating the good miscibility of PBDTTT-C-T and PBDTTPD. This may be ascribed to the structural similarity of the two donors. The 珡lm morphologies with different PBDTTT-C-T contents investigated by AFM are shown in Fig. S2 in the ESI.† These 珡lms present different grain sizes. Small grains were found when incorporating 30% of PBDTTT-C-T into the ternary blend 珡lm. Relatively large grains appear when 50% or 70% of PBDTTT-C-T is added into the ternary blend. The grain size may in珞uence phase separation and furthermore the performance of the devices. In order to depict the blend morphology throughout the active layer, the bulk morphologies of the 珡lms were investigated by transmission electron microscopy (TEM). The two binary 珡lms show similar bulk morphologies consist- ing of thin, 珡bre-like features (Fig. 4g and i). However, relatively large domain sizes and remarkable phase separation are observed when the PBDTTT-C-T content is larger than that of PBDTTPD (Fig. S2i†), which lead to the poorer photovoltaic performances.

As shown in Fig. 5, the stacking of the active layers in the out-of-plane direction was studied by X-ray diffraction (XRD, Bruker D8). To further verify the molecular orientation, two-dimensional grazing-incidence X-ray diffraction (2D GIXD, at beamline BL14B1) was performed in the in-plane direction.[24] The PBDTTPD:$PC_{71}BM$ and PBDTTT-C-T:$PC_{71}BM$ 珡lms have almost the same diffraction peak positions at *ca.* 4.5°, which is attributed to the (100) lattice plane. The diffraction peak of the (010) lattice plane is only found in the PBDTTPD:$PC_{71}BM$ 珡lm, which indicates that face-on orientations are formed in this blend. The ternary blend 珡lms show the same peak at 4.5°.

Although the intensities decrease gradually with the increase of the PBDTTT-C-T content in ternary active layers, the 珡lms still retain their high crystallinity. This may be caused by the structural similarity of PBDTTT-C-T with PBDTTPD. Moreover, the (010) peak is found when adding 30% PBDTTT-C-T, but it disappears when adding 50% PBDTTT-C-T. For the 2D GIWAXS measurements in the in-plane direction, the (100) peaks are found in both binary and ternary blends, which indicates that the PBDTTPD and PBDTTT-C-T prefer face-on molecular orientations, which tend to bene珡t hole transport in blend 珡lms.[24]

In this ternary PSC, the V_{oc} increases linearly with the increase of the PBDTTT-C-T content.[24,26,38] This is different from some reports on ternary blend OSCs, in which the V_{oc} is limited by the lower value of the binary systems. It is known that the V_{oc} is determined by the offset of the HOMO of donors and the LUMO of the acceptor. Thus UPS measurements were employed to estimate the HOMO of the blend of PBDTTPD:PBDTTT-C-T (7 : 3). PBDTTT-C-T and PBDTTPD were also measured for comparison (Fig. 6).[37] According to the UPS results, the HOMO values of PBDTTPD, PBDTTT-C-T and the blend are around —5.35 eV, —5.08 eV and —5.21 eV, respectively. The changes of V_{oc} can be ascribed to the formation of new energy levels in the ternary blends, each of which exhibits only one energy level other than the two initial energy levels of PBDTTPD and PBDTTT-C-T. We note that the V_{oc} of the ternary devices concentrates in the range of 0.81–0.85 V. This can be explained by the concept of formation of an alloy structure. The similar structures of the two donor materials, associated with the morphology and XRD results, indicate that PBDTTPD and PBDTTT-C-T should be well-mixed. Thus, the electrical properties of PBDTTPD can be easily affected by PBDTTT-C-T, even with a very low PBDTTT-C-T content of 10%.[24,37]

To investigate whether there is energy transfer between PBDTTPD and PBDTTT-C-T, the photoluminescence (PL) of PBDTTPD, PBDTTT-C-T and PBDTTPD:PBDTTT-C-T (weight ratio of 7 : 3) in 珡lms was measured. As shown in Fig. 7, the PBDTTPD 珡lm exhibits strong PL around 660 nm, whereas the PBDTTT-C-T 珡lm shows a relatively lower PL around 750 nm. The PBDTTPD:PBDTTT-C-T (7 : 3) blend 珡lm presents clearly higher PL intensity as compared to the neat PBDTTT-C-T 珡lm,

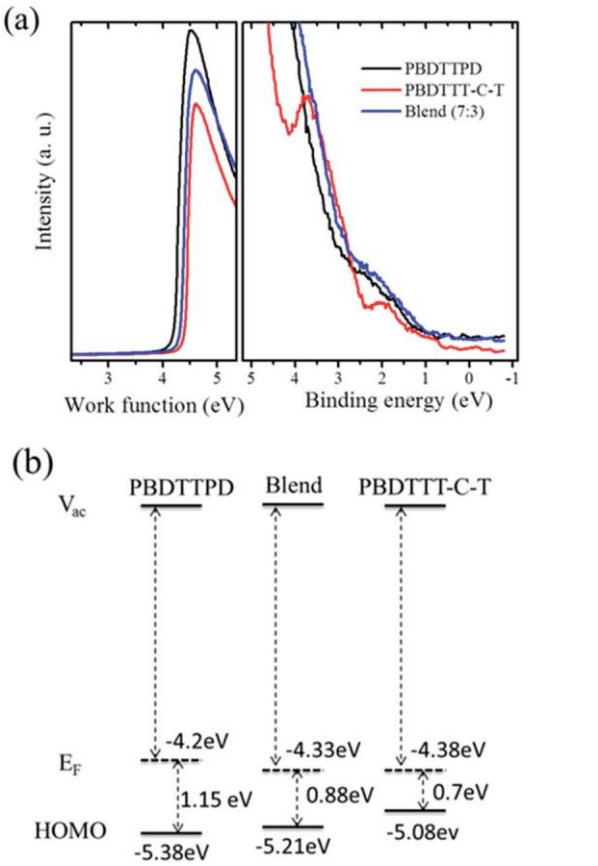

Fig. 6 (a) Secondary electron cut-offs of the UPS (left) and onsets of the HOMO peaks (right) of the neat PBDTTPD and PBDTTT-C-T films, and the PBDTTPD:PBDTTT-C-T blend film with a weight ratio of 7 : 3. (b) HOMO levels obtained from the UPS results.

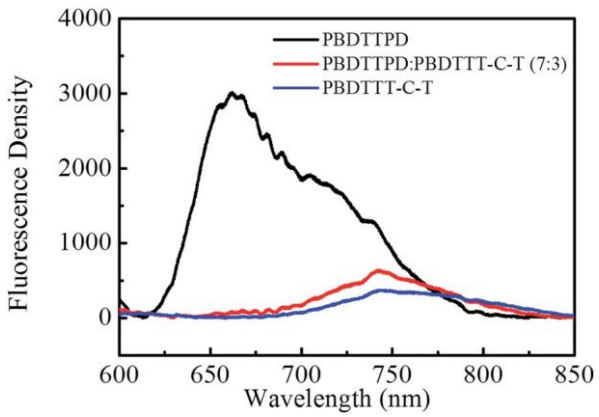

Fig. 7 Photoluminescence spectra of the neat PBDTTPD and PBDTTT-C-T films and PBDTTPD:PBDTTT-C-T (7 : 3) blend film.

while the PL of PBDTTPD completely disappears. This indicates that excitons can be transferred from PBDTTPD to PBDTTT-C-T, resulting in the enhanced PL of PBDTTT-C-T in the blend 珡lm. In addition, we note that the PL of PBDTTPD and the absorption of PBDTTT-C-T are overlapped, which is the prerequisite for efficient energy transfer from PBDTTPD to PBDTTT-C-T.[26,40]

3. Conclusions

A high-performance ternary PSC is developed by using two polymers PBDTTT-C-T and PBDTTPD as donors and $PC_{71}BM$ as the acceptor. With the optimized PBDTTPD:PBDTTT-C-T:$PC_{71}BM$ ratio of 0.7 : 0.3 : 1.5, the ternary PSC demonstrates a higher PCE of 9.3% as compared to the two binary PSCs as reference. The enhanced J_{sc} of the ternary PSC stems from the extended light absorption. The similar polymer structures of PBDTTPD and PBDTTT-C-T promote good miscibility and the desired morphology in the ternary blend 珡lm. The changes of V_{oc} can be explained by the electronic alloy concept, which is con珡rmed by XRD and UPS measurements. This work demonstrates that using structurally similar donor polymers with complementary absorption is a rational strategy to achieve high-performance ternary PSCs.

4. Experimental

Materials

PBDTTT-C-T and $PC_{71}BM$ (99.5%) were purchased from Solarmer and American Dye Sources Inc, respectively, and PBDTTPD was synthesized by following the literature.[39]

PSC fabrication

The detailed device fabrication processes are as follows: ITO-coated glass substrates with a nominal sheet resistance of 15 U per square were ultrasonically cleaned for 20 min with detergent, de-ionized water, acetone and iso-propyl alcohol, respectively. A洐er drying under N_2 珠ow, the substrates were treated with O_2 Plasma 珠ow for 6 min (Plasmon Preen II-862, Mycro Co.) prior to the deposition of the PEDOT:PSS layer. The PEDOT:PSS solution (Clevios PVP Al4083, HC Starck) was spin-coated with a speed of 4000 rpm for 40 s and then annealed at 160 °C for 20 min. The thickness of the PEDOT:PSS layer was about 40 nm. A洐er thermal annealing, the substrates covered with PEDOT:PSS were transferred into a nitrogen-珡lled glovebox to spin-coat the active layer. The active layer materials were beforehand dissolved in chlorobenzene (CB) solution with a donor and acceptor mass ratio of 1 : 1.5 and a polymer concentration of 10 mg ml^{-1} 5 vol% 1-chloronaphthalene (CN) and 3 vol% 1,8-diiodooctane (DIO) were simultaneously added to the solution mixture to act as the morphology optimizing reagent of the active layer. Different volume ratios of PBDTTPD:$PC_{71}BM$ and PBDTTT-C-T:$PC_{71}BM$ CB solutions were mixed together to obtain ternary donor containing solution mixtures with various mass ratios and the mixed solutions were stirred for 10 minutes before spin-coating to mix them homogenously. The thickness of the active layer in the ternary device is about 100 nm. Finally, Ca and Al metallic particles were thermally evaporated onto the active layer with a thickness of 10 nm and 100 nm respectively, to form the cathode under vacuum (#10^{-6} Torr) conditions, and the whole active layer area of the device was 0.1 cm^2 controlled by a shadow mask for all OPV devices in this work. The current density–voltage (J–V) characteristics of the OPVs were measured under AM 1.5G solar irradiation, at 100 mW cm^{-2}. The external quantum efficiencies

(EQE) of the OPVs were analyzed by using a certified Newport incident photon conversion efficiency (IPCE) measurement system.

Characterization

The UV-Vis-NIR absorption spectra of the active layers were recorded on a Varian Cary 50 UV-Vis spectrometer. The X-ray diffraction (XRD) spectra were measured using a Bruker D8. Two-dimensional grazing-incidence X-ray diffraction (2D GIXD) was performed at beamline BL14B1 (Shanghai Synchrotron Radiation Facility). Atomic force microscopy (AFM) measurements were carried out on an Agilent 5400 AFM at ambient temperature. The transmission electron microscopy (TEM) images of the active layers were obtained on a JEM-2000 Ex. Ultraviolet Photoelectron Spectrometer (UPS) measurements were carried out on an ESCALAB 250Xi from Thermo Scientific.

Acknowledgements

This work was supported by the National Natural Science Foundation of China (61405209, 51573205, and 21604092) and Ministry of Science and Technology of China (2014CB643501 and 2010DFA52310). The authors thank beamline BL14B1 (Shanghai Synchrotron Radiation Facility) for providing the beam time.

Notes and references

1 A. J. Heeger, *Adv. Mater.*, 2014, 26, 10–28.
2 S. Günes, H. Neugebauer and N. S. Sariciftci, *Chem. Rev.*, 2007, 107, 1324–1338.
3 T. M. Clarke and J. R. Durrant, *Chem. Rev.*, 2010, 110, 6736–6767.
4 H. Kang, G. Kim, J. Kim, S. Kwon, H. Kim and K. Lee, *Adv. Mater.*, 2016, 28, 7821–7861.
5 L. Dou, J. You, Z. Hong, Z. Xu, G. Li, R. A. Street and Y. Yang, *Adv. Mater.*, 2013, 25, 6642–6671.
6 Y. Liu, J. Zhao, Z. Li, C. Mu, W. Ma, H. Hu, K. Jiang, H. Lin, H. Ade and H. Yan, *Nat. Commun.*, 2014, 5, 5293.
7 W. Zhao, D. Qian, S. Zhang, S. Li, O. Inganäs, F. Gao and J. Hou, *Adv. Mater.*, 2016, 28, 4734–4739.
8 J. Zhao, Y. Li, A. Hunt, J. Zhang, H. Yao, Z. Li, J. Zhang, F. Huang, H. Ade and H. Yan, *Adv. Mater.*, 2016, 28, 1868–1873.
9 H. Hu, K. Jiang, G. Yang, J. Liu, Z. Li, H. Lin, Y. Liu, J. Zhao, J. Zhang, F. Huang, Y. Qu, W. Ma and H. Yan, *J. Am. Chem. Soc.*, 2015, 137, 14149–14157.
10 S. Li, L. Ye, W. Zhao, S. Zhang, S. Mukherjee, H. Ade and J. Hou, *Adv. Mater.*, 2016, 28, 9423–9429.
11 H. Hoppea and N. S. Sariciftci, *J. Mater. Res.*, 2004, 19, 1924–1945.
12 J. You, L. Dou, K. Yoshimura, T. Kato, K. Ohya, T. Moriarty, K. Emery, C.-C. Chen, J. Gao and G. Li, *Nat. Commun.*, 2013, 4, 1446.
13 J. You, C. C. Chen, Z. Hong, K. Yoshimura, K. Ohya, R. Xu, S. Ye, J. Gao, G. Li and Y. Yang, *Adv. Mater.*, 2013, 25, 3973–3978.
14 T. Liu, Y. Guo, Y. Yi, L. Huo, X. Xue, X. Sun, H. Fu, W. Xiong, D. Meng, Z. Wang, F. Liu, T. P. Russell and Y. Sun, *Adv. Mater.*, 2016, 28, 10008–10015.
15 L. Nian, K. Gao, F. Liu, Y. Kan, X. Jiang, L. Liu, Z. Xie, X. Peng, T. P. Russell and Y. Ma, *Adv. Mater.*, 2016, 28, 8184–8190.
16 W. Zhao, S. Li, S. Zhang, X. Liu and J. Hou, *Adv. Mater.*, 2017, 29, 1604059.
17 J. Zhao, Y. Li, G. Yang, K. Jiang, H. Lin, H. Ade, W. Ma and H. Yan, *Nat. Energy*, 2016, 1, 15027.
18 Q. An, F. Zhang, J. Zhang, W. Tang, Z. Deng and B. Hu, *Energy Environ. Sci.*, 2016, 9, 281–322.
19 T. Ameri, P. Khoram, J. Min and C. J. Brabec, *Adv. Mater.*, 2013, 25, 4245–4266.
20 W. Chen, M. Xiao, L. Han, J. Zhang, H. Jiang, C. Gu, W. Shen and R. Yang, *ACS Appl. Mater. Interfaces*, 2016, 8, 19665–19671.
21 L. Lu, T. Zheng, Q. Wu, A. M. Schneider, D. Zhao and L. Yu, *Chem. Rev.*, 2015, 115, 12666–12731.
22 H. Zhou, Y. Zhang, C.-K. Mai, S. D. Collins, G. C. Bazan, T.-Q. Nguyen and A. J. Heeger, *Adv. Mater.*, 2015, 27, 1767–1773.
23 L. Lu, T. Xu, W. Chen, E. S. Landry and L. Yu, *Nat. Photonics*, 2014, 8, 716–722.
24 J. Zhang, Y. Zhang, J. Fang, K. Lu, Z. Wang, W. Ma and Z. Wei, *J. Am. Chem. Soc.*, 2015, 137, 8176–8183.
25 N. Gasparini, X. Jiao, T. Heumueller, D. Baran, G. J. Matt, S. Fladischer, E. Spiecker, H. Ade, C. J. Brabec and T. Ameri, *Nat. Energy*, 2016, 1, 16118.
26 V. Gupta, V. Bharti, M. Kumar, S. Chand and A. J. Heeger, *Adv. Mater.*, 2015, 27, 4398–4404.
27 H. Lu, J. Zhang, J. Chen, Q. Liu, X. Gong, S. Feng, X. Xu, W. Ma and Z. Bo, *Adv. Mater.*, 2016, 28, 9559–9566.
28 F. Bonaccorso, N. Balis, M. M. Stylianakis, M. Savarese, C. Adamo, M. Gemmi, V. Pellegrini, E. Stratakis and E. Kymakis, *Adv. Funct. Mater.*, 2015, 25, 3870–3880.
29 H. Cha, D. S. Chung, S. Y. Bae, M.-J. Lee, T. K. An, J. Hwang, K. H. Kim, Y.-H. Kim, D. H. Choi and C. E. Park, *Adv. Funct. Mater.*, 2013, 23, 1556–1565.
30 P. P. Khlyabich, A. E. Rudenko, B. C. Thompson and Y.-L. Loo, *Adv. Funct. Mater.*, 2015, 25, 5557–5563.
31 N. Gasparini, M. Salvador, S. Fladischer, A. Katsouras, A. Avgeropoulos, E. Spiecker, C. L. Chochos, C. J. Brabec and T. Ameri, *Adv. Energy Mater.*, 2015, 5, 1501527.
32 S.-J. Ko, W. Lee, H. Choi, B. Walker, S. Yum, S. Kim, T. J. Shin, H. Y. Woo and J. Y. Kim, *Adv. Energy Mater.*, 2015, 5, 1401687.
33 T. H. Lee, M. A. Uddin, C. Zhong, S.-J. Ko, B. Walker, T. Kim, Y. J. Yoon, S. Y. Park, A. J. Heeger, H. Y. Woo and J. Y. Kim, *Adv. Energy Mater.*, 2016, 6, 1600637.
34 T. Liu, L. Huo, X. Sun, B. Fan, Y. Cai, T. Kim, J. Y. Kim, H. Choi and Y. Sun, *Adv. Energy Mater.*, 2016, 6, 1502109.
35 S. A. Mollinger, K. Vandewal and A. Salleo, *Adv. Energy Mater.*, 2015, 5, 1501335.
36 W. Chen, Z. Du, M. Xiao, J. Zhang, C. Yang, L. Han, X. Bao and R. Yang, *ACS Appl. Mater. Interfaces*, 2015, 7, 23190–23196.

37 T. Yang, M. Wang, C. Duan, X. Hu, L. Huang, J. Peng, F. Huang and X. Gong, *Energy Environ. Sci.*, 2012, 5, 8208.
38 N. Felekidis, E. Wang and M. Kemerink, *Energy Environ. Sci.*, 2016, 9, 257–266.
39 C. Cabanetos, A. El Labban, J. A. Bartelt, J. D. Douglas, W. R. Mateker, J. M. Frechet, M. D. McGehee and P. M. Beaujuge, *J. Am. Chem. Soc.*, 2013, 135, 4656–4659.
40 S. Zhang, L. Zuo, J. Chen, Z. Zhang, J. Mai, T.-K. Lau, X. Lu, M. Shi and H. Chen, *J. Mater. Chem. A*, 2016, 4, 1702–1707.
41 M. Ghasemi, L. Ye, Q. Zhang, L. Yan, J. H. Kim, O. Awartani, W. You, A. Gadisa and H. Ade, *Adv. Mater.*, 2017, 29, 1604603.
42 L. Zhong, L. Gao, H. Bin, Q. Hu, Z. G. Zhang, F. Liu, T. P. Russell, Z. Zhang and Y. Li, *Adv. Energy Mater.*, 2017, 7, 1602215.
43 F. Zhao, Y. Li, Z. Wang, Y. Yang, Z. Wang, G. He, J. Zhang, L. Jiang, T. Wang, Z. Wei, W. Ma, B. Li, A. Xia, Y. Li and C. Wang, *Adv. Energy Mater.*, 2017, 7, 1602552.
44 T. Goh, J.-S. Huang, B. Bartolome, M. Y. Sfeir, M. Vaisman, M. L. Lee and A. D. Taylor, *J. Mater. Chem. A*, 2015, 3, 18611–18621.
45 J. Mai, H. Lu, T.-K. Lau, S.-H. Peng, C.-S. Hsu, W. Hua, N. Zhao, X. Xiao and X. Lu, *J. Mater. Chem. A*, 2017, DOI: 10.1039/C7TA00292K.
46 L. Xiao, K. Gao, Y. Zhang, X. Chen, L. Hou, Y. Cao and X. Peng, *J. Mater. Chem. A*, 2016, 4, 5288–5293.
47 T. Ameri, J. Min, N. Li, F. Machui, D. Baran, M. Forster, K. J. Schottler, D. Dolfen, U. Scherf and C. J. Brabec, *Adv. Energy Mater.*, 2012, 2, 1198–1202.
48 T. Ameri, T. Heumüller, J. Min, N. Li, G. Matt, U. Scherf and C. J. Brabec, *Energy Environ. Sci.*, 2013, 6, 1796–1801.
49 T. Ameri, P. Khoram, T. Heumuller, D. Baran, F. Machui, A. Troeger, V. Sgobba, D. Guldi, M. Halik and S. Rathgeber, *J. Mater. Chem. A*, 2014, 2, 19461–19472.
50 H. Huang, L. Yang and B. Sharma, *J. Mater. Chem. A*, 2017, DOI: 10.1039/C7TA00887B.
51 L. Lu, W. Chen, T. Xu and L. Yu, *Nat. Commun.*, 2015, 6, 7327.
52 J. Mai, T. K. Lau, J. Li, S. H. Peng, C. S. Hsu, U. Jeng, J. Zeng, N. Zhao, X. Xiao and X. Lu, *Chem. Mater.*, 2016, 28, 6186–6195.
53 N. Gasparini, L. Lucera, M. Salvador, M. Prosa, G. D. Spyropoulos, P. Kubis, H. J. Egelhaaf, C. J. Brabec and T. Ameri, *Energy Environ. Sci.*, 2017, 10, 885–892.
54 Y. Yang, W. Chen, L. Dou, W.-H. Chang, H.-S. Duan, B. Bob, G. Li and Y. Yang, *Nat. Photonics*, 2015, 9, 190–198.
55 L. Huo, S. Zhang, X. Guo, F. Xu, Y. Li and J. Hou, *Angew. Chem., Int. Ed.*, 2011, 50, 9697–9702.